SCIENTIFIC REPORTS

OPEN

Vacuum level dependent photoluminescence in chemical vapor deposition-grown monolayer MoS_2

Received: 17 May 2017
Accepted: 30 October 2017
Published online: 01 December 2017

Linfeng Sun[1,2], Xiaoming Zhang[1], Fucai Liu[3], Youde Shen[4], Xiaofeng Fan[5], Shoujun Zheng[2], John T. L. Thong[4], Zheng Liu[3,6], Shengyuan A. Yang[1] & Hui Ying Yang[1]

The stronger photoluminescence (PL) in chemical vapor deposition (CVD) grown monolayer MoS_2 has been attributed to its high crystal quality compared with that in mechanically exfoliated (ME) crystal, which is contrary to the cognition that the ME crystal usually have better crystal quality than that of CVD grown one and it is expected with a better optical quality. In this report, the reason of abnormally strong PL spectra in CVD grown monolayer crystal is systematically investigated by studying the *in-situ* opto-electrical exploration at various environments for both of CVD and ME samples. High resolution transmission electron microscopy is used to investigate their crystal qualities. The stronger PL in CVD grown crystal is due to the high p-doping effect of adsorbates induced rebalance of exciton/trion emission. The first principle calculations are carried out to explore the interaction between adsorbates in ambient and defects sites in MoS_2, which is consistent to the experimental phenomenon and further confirm our proposed mechanisms.

Transition metal dichalcogenides (TMDs) have attracted tremendous attention due to their extraordinary opto-electrical properties, setting the stage for new breakthroughs in materials science, especially when the thickness of these materials approaches atomic-level thicknesses[1–7]. Molybdenum disulfide (MoS_2), as a typical TMD, has experimentally demonstrated high mobility and high on/off ratio when used as an active material in electronics devices, while the circularly polarized photoluminescence (PL) for single layer MoS_2 makes it promising for valleytronic devices[7–10]. Though single layer MoS_2 is a good candidate for its application in electronic devices, the size of samples fabricated by ME method limits its practical use. Therefore, CVD method has been used to synthesize large-area samples although the electrical properties of CVD grown samples are poorer than that of ME samples[11–15]. However, CVD grown monolayer MoS_2 displays abnormally optical quality with a stronger PL intensity compared to that of ME samples, which has been observed in previous reports and attributed to the proof of high crystal quality[16,17], since optical performance at room temperature is usually used to evaluate the crystal quality of two dimensional (2D) semiconductors, based on the premise that intense PL emission is observed for low-defective compound semiconductors[18]. However, this conclusion cannot work here, because the crystal quality of ME samples is usually better than that of CVD grown samples and is expected with a better optical quality. Till now, it is still a controversial issue that the precious explanation for the stronger PL in CVD grown samples than that of ME sample is due to its higher crystal quality[16,17,19–23]. Thus, the mechanism for the strong PL in CVD grown samples is still lacking and the clarification for this doubt in this work will be desirable and helpful to recognize its nature of stronger PL in CVD grown samples. In this work, by investigating the optical

[1]Pillar of Engineering Product Development, Singapore University of Technology and Design, Singapore, 487372, Singapore. [2]Division of Physics and Applied Physics, School of Physical and Mathematical Science, Nanyang Technological University, Singapore, 637371, Singapore. [3]Center for Programmable Materials, School of Materials Science and Engineering, Nanyang Technological University, Singapore, 639798, Singapore. [4]Department of Electrical and Computer Engineering, National University of Singapore, Singapore, 117583, Singapore. [5]College of Materials Science and Engineering, Jilin University, Changchun, 130012, P. R. China. [6]Centre for Micro-/Nano-electronics (NOVITAS), School of Electrical & Electronic Engineering, Nanyang Technological University, Singapore, 639798, Singapore. Correspondence and requests for materials should be addressed to H.Y.Y. (email: yanghuiying@sutd.edu.sg)

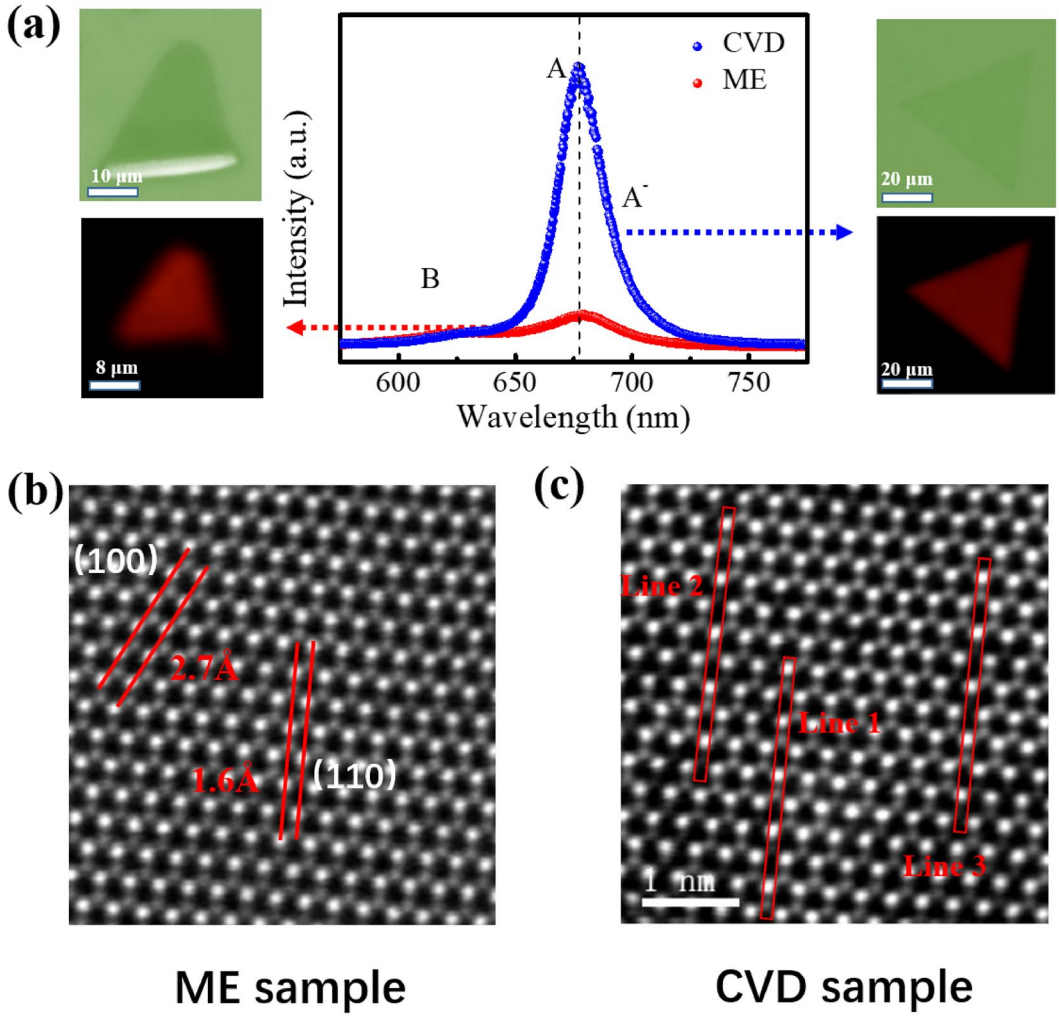

Figure 1. (**a**) PL spectra of single layer ME and CVD grown MoS_2. Left column: optical image of a typical monolayer sample fabricated by ME method and its PL mapping. Right column: optical image of a typical CVD-grown monolayer sample and its PL mapping. Both of two PL mappings are normalized to the intensity of A exciton. (**b**) and (**c**) are the HAADF image of ME and CVD samples, respectively. The lines indicate the defects observed in this image.

spectra of monolayer MoS_2 samples with different amounts of defects, as well as their electrical performance, we uncover the emission mechanism of abnormally strong PL observed in CVD grown samples and attribute it to the p doping effect from the larger amounts of adsorbates on the defect sites of MoS_2, which rebalance the radiative emission intensities of excitons.

Results and Discussion

Figure 1a shows the PL spectra of typical CVD grown and ME monolayer MoS_2. Their corresponding PL mappings show the uniform intensities. Clearly, the PL intensity of the former is stronger than that of the latter, which was previously attributed to the high crystal quality of CVD grown crystal[16,17]. The X-ray photoelectron spectroscopies for these two groups of samples are carried out to show the atomic ratio (S/Mo), as shown in Fig. S1. For CVD grown sample, the peaks at 162.3 and 163.4 eV are assigned to the S^{2-} $2p_{3/2}$ and $2p_{1/2}$, respectively. The peaks at 229.5 and 232.7 eV are attributed to the Mo^{4+} $3d_{5/2}$ and $3d_{3/2}$. While for ME sample, the peaks at 162.6 and 163.6 eV are assigned to the 2p3/2 and 2p1/2, of divalent sulphide ions (S^{2-}) and the peaks at 229.67 and 232.8 eV are from the $3d_{5/2}$ and $3d_{3/2}$ of the core levels of Mo^{4+}. The S/Mo ratio for CVD sample is 1.66 and that for ME sample is 1.86, which is consistent to the results of EDS and more defects are introduced in CVD grown samples. Figure 1b,c show typical high resolution atomic structure generated by high angle annular dark field (HAADF) scanning transmission electron microscopy (STEM), and they clearly display the defects in CVD grown monolayer MoS_2, as indicated in the lines. The lattice spaces of hexagonal lattice structure for MoS_2 is 2.7 Å ((100) plane) and 1.6 Å ((110) plane). The corresponding intensity line profiles shows in Fig. S2 display most of defects are single S vacancy. Fig. S3a gives a directly visual sense of the effect of defects on the PL intensities of ME MoS_2. The marked circle area with pre-exposed by Argon (Ar) plasma shows stronger PL intensity. Fig. S3b shows the PL spectra of area A (exposed by Ar plasma) and B (without Ar plasma treatment), respectively. Therefore, it

seems that the more defects contribute to the stronger PL emission in MoS_2. Nevertheless, whether the PL spectra observed in MoS_2 is its intrinsic emission or defect-induced emission remains unclear. The previous reports have revealed the energy of defect-induced PL is around 1.78 eV, at the low energy side of the reported A exciton[22]. However, as shown in Fig. 1, there is no extra emission peak except a broadened shoulder, which has been identified as the trion emission, marked as A^- exciton emission. Moreover, the temperature dependent PL spectra (shown in Fig. S4) indicates the PL peak observed is an intrinsic emission, and the match among the electron spin, the layer pseudospin and the valley pseudospin reported in the literature display the features of intrinsic emission[6–9,24]. Thus the observed PL peak in Fig. 1 is not the defect-induced emission in MoS_2. Another potential factor that may lead to the difference of optical properties between CVD grown and ME samples is the strain effect from the substrate since the contact behaviours between the substrate and the sample are different for these two cases. The CVD grown samples are inevitably affected by the strain effect because of the different thermal expansion coefficients between deposited layer and substrate during the cooling process[25–27]. Figure S5 compares the Raman spectra of both of CVD grown and ME sample. The E^1_{2g} and A_{1g} modes of CVD grown samples show a red-shift and blue-shift, respectively, when compared with those of ME 1 L MoS_2 sample. This phenomenon differs from the variation trend when strain is applied[28]. Also, if the strain effect is the main factor in the PL spectra of MoS_2, the energies of PL would shift clearly towards higher energy (compressive strain) and lower energy (tensile strain), respectively[29,30], but there is no obvious shift of peak position shown in Fig. 1. Thus, the strain effect could be excluded in this study. So far, defects are most likely to be responsible for the enhancement of photon emission in CVD grown monolayer MoS_2.

Since defects in atomically layered materials usually could act as adsorption centres due to their higher active adsorption energy, the PL spectra of CVD and ME MoS_2 sample were measured in vacuum to exclude the role of adsorbates. Surprisingly, as shown in Fig. 2a, the PL intensity of CVD grown MoS_2 decreased dramatically in vacuum. At the same time, the emission intensities are reversible when the CVD grown samples exposed in air again. However, for the PL spectra of ME sample (Fig. 2b), its intensity does not show obvious variations with the ambient varies. The reduction of PL intensity in vacuum for CVD grown sample implies that the adsorbates adsorbed on the surface of MoS_2 greatly affect its photon emission. According to the vacuum-level dependent PL intensities, it seems that more adsorbates contribute to stronger PL intensity. Moreover, it is found that in Fig. 2c, the ratio of PL intensities between CVD grown and ME MoS_2 samples is even less than 1 when the adsorbates level is at the lowest vacuum level (1×10^{-5} mbar). This result shows that the PL intensity of CVD grown sample is comparable or even weaker than that of ME sample, which verifies that the room-temperature optical performance in vacuum could reflect the crystal quality. Figure 2d,e show the PL images of a typical CVD grown sample with grain boundary in air and vacuum, respectively. The sites at the grain boundary are expected with more defects and its decreased PL intensity measured in vacuum provides clear evidence that PL intensities at defect sites could be decreased when measured in vacuum.

Meanwhile, the *in-situ* Raman spectra have been obtained for these two groups of MoS_2 samples, as shown in Fig. S6. There is no obvious change for the E^1_{2g} mode (almost fixed at ~385.7 cm^{-1} for ME sample and ~384.4 for CVD grown sample), but a clear blue-shift of A_{1g} mode (from 404.94 cm^{-1} to 403.35 cm^{-1}) for the CVD sample in vacuum compared with that in air, shown in Fig. S6a, which is larger than that of ME sample with a smaller shift from 404.21 cm^{-1} to 403.71 cm^{-1} (Fig. S6b). This result is different from the reported strain effect on the Raman spectra for monolayer MoS_2 sample[28], which could be further exclude the strain effect. The similar variation trends for A_{1g} and E^1_{2g} mode have been reported by the gated Raman spectra from a 1 L MoS_2[31]. The results show the softening of the A_{1g} mode with electron doping, while the frequency of E^1_{2g} mode remains unchanged, which are due to the stronger electron-phonon coupling of the A_{1g} mode than that of the E^1_{2g} mode[32,33]. So whether the shift of A_{1g} modeobserved in this work is due to the doping effect will be discussed later.

The vacuum-level dependent electrical performances of CVD grown and ME MoS_2 are investigated. Figure 3a shows the schematic of a monolayer MoS_2 based transistor fabricated in this work. The fabrication process is described in the experimental section. The optical images of FETs based on ME and CVD grown samples are shown in Fig. S7. Figure 3b,c show the electrical performance of single layer ME and CVD grown MoS_2 based transistors, respectively. Both of these two groups transistors display n type behaviour, which mean excess electrons introduced in MoS_2. Moreover, with the vacuum level decreasing, the threshold voltage shifts towards the positive direction, which means that the adsorbates in air play a p doping effect on MoS_2 itself. Additionally, comparing the current at $V_g = 0$ V, the current is larger under vacuum when compared with that in air, which represents a stronger n doped effect in vacuum. While in air, due to the p doping effect from absorbates, the current is decreased. Both of CVD grown and ME samples show this variation trend. The mobility for CVD grown samples in vacuum is 0.69 cm^2/VS while it is 44.2 cm^2/VS for ME samples in vacuum, which means a poor crystal quality for CVD grown samples without doping effect from adsorbates. While this p-doping effect due to the adsorbates in air reduced the amounts of the excess electron in MoS_2 and thus increased the radiative decay of exciton emission, which could be described by a three-level model including the excitation, exciton emission and trion emission processes[4,34]. As shown in Fig. S8a, G represents the generation rate of optical excitons. The radiative decay rates of the exciton and trion are marked as Γ_{ex} and Γ_{tr} respectively. When the mass action law is considered with trions together to evaluate the doped electron density in MoS_2 samples, the integrated intensity ratio of trion emission (I_{tr}) to electron emission (I_{ex}) can be expressed as[34–37]:

$$\frac{I_{tr}}{I_{ex}} = \propto \frac{n_e}{k_b T} \tag{1}$$

I_{tr} and I_{ex} represent the trion and exciton emission intensities, respectively. n_e is the carrier concentration, k_b is the Boltzmann constant, and T represents temperature.

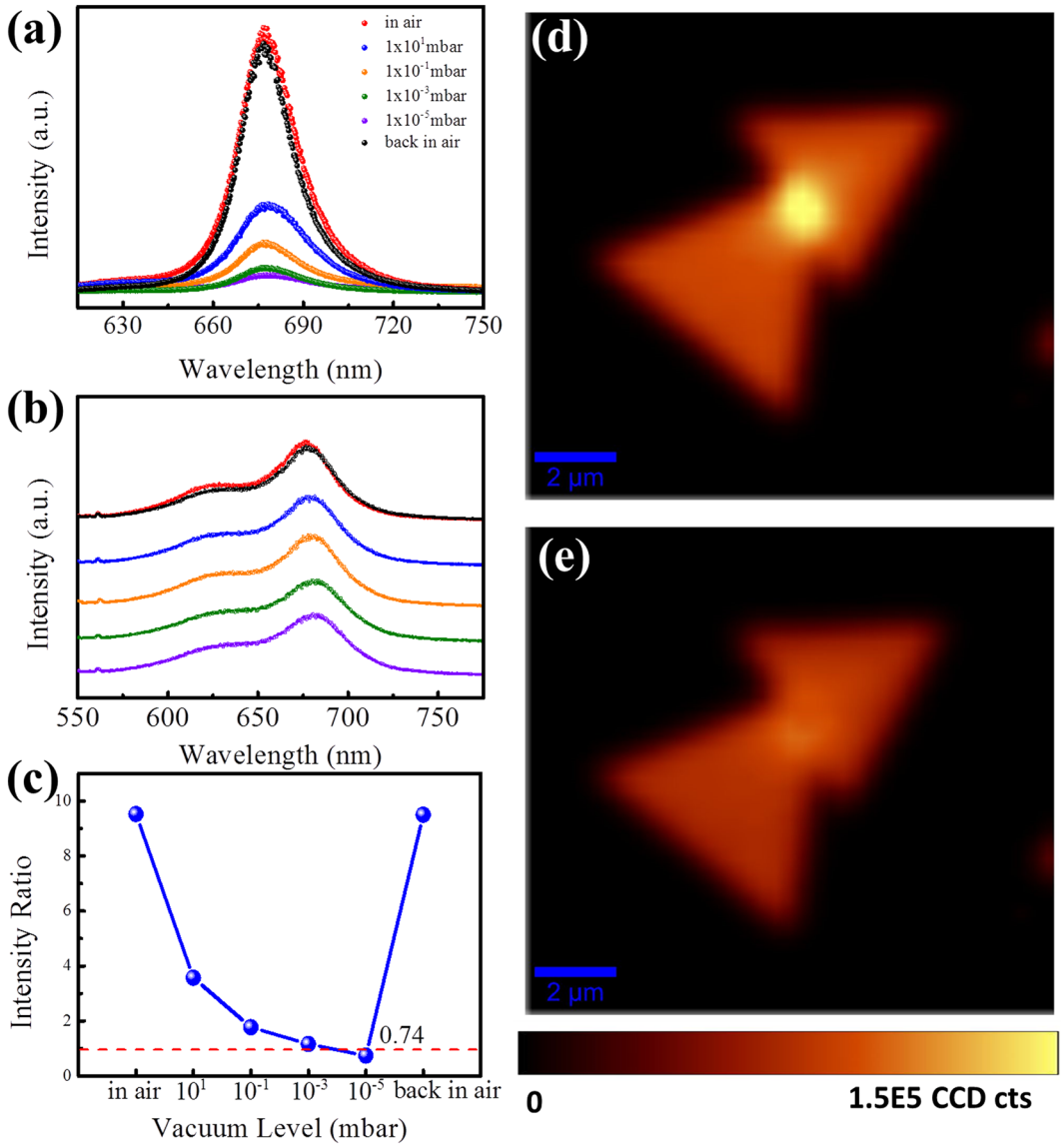

Figure 2. Vacuum level dependent PL spectra of (**a**) CVD grown and (**b**) ME MoS_2 samples. (**c**) The ratios of PL intensities between CVD grown and ME MoS_2 samples at different vacuum levels shown in Figure (**a**,**b**). The PL mappings of a typical CVD-grown monolayer MoS_2 measured in air (**d**) and vacuum (**e**), respectively. Both of PL mappings are normalized to the intensity of A exciton.

From equation (1), it is confirmed that the ratio of emission intensities from I_{tr} and I_{ex} indeed highly depends on the carrier concentration in MoS_2, which corresponds to the experimental results shown in Fig. S8b. The fitting results for CVD grown and ME samples in air and vacuum are shown in Fig. S9, respectively, which directly reflect the vacuum level dependent intensity ratio of exciton and trion. Moreover, it is concluded that the binding energy of trion is ~24 meV. So their emission spectra overlapped with that of exciton emission since such negatively charged excitons usually have finite binding energies, ~20 meV[4].

Moreover, such a p doing effect also explain well the Raman frequency shift of E^1_{2g} and A_{1g} mode observed in Fig. S6. According to the symmetrical group theory, the A_{1g} mode has symmetrical lattice variation and would have a nonzero expectation value for the matrix element of the electron-phonon coupling, which leads to a larger electron-phonon coupling[31]. While for the E^1_{2g} mode, the matric element of electron phonon coupling vanishes and its coupling with electrons is weaker on doping in ambient compared with A_{1g} modes[31–33]. Moreover, we have calculated the phonon energies of E^1_{2g} mode and A_{1g} mode with and without considering the adsorbates, as shown in Fig. S10, the results are consistent to our experimental results and explanation above.

So far, the physical picture for the reason why the CVD grown sample shows a strong PL intensity is clear. The greater the amounts of adsorbates, the stronger the intensity of the PL emission in MoS_2. Supposing there is no adsorption on the surface of MoS_2, the PL intensity from CVD grown MoS_2 should be weaker than that of ME sample due to its poorer crystal quality, which is corresponding to the experimental results on the intensity ratio (0.74) at higher vacuum shown in Fig. 2c.

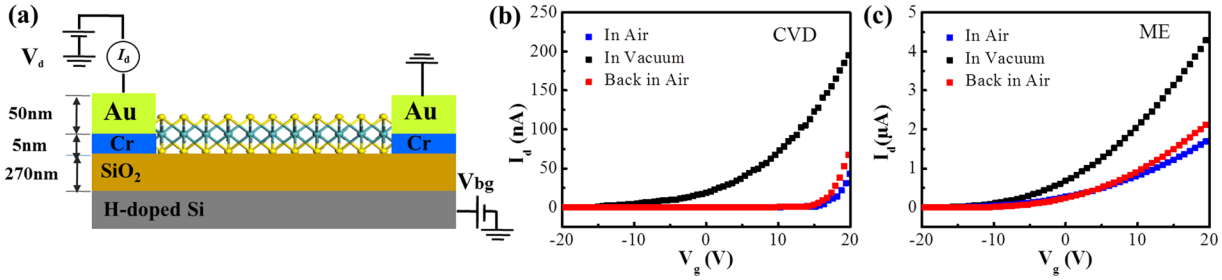

Figure 3. (**a**) The schematic of transistors used in this work. I_d -V_g curves of (**b**) CVD grown and (**c**) ME MoS_2 transistors for $V_{bg} = -20$ V to 20 V measured in air, vacuum, and back to air, respectively. The fixed source-drain voltage is 1 V. The black, blue and red colour lines represent the curves measured in vacuum, air and back to air, respectively.

Furthermore, the CVD grown monolayer MoS_2 under different growth conditions marked as S1, S2, S3, S4, and S5, respectively, are investigated to confirm the vacuum level dependent PL spectra. Figure 4a shows the optical images of selected CVD samples. Their PL intensities are different in air (Fig. 4b), and their emission intensities are reduced measured in vacuum (1×10^{-5} mbar) by different extent, as shown in Fig. 4c. Figure 4d presents the ratios of PL intensities measured in air and vacuum for these samples. The different ratios when the vacuum level varies during measurement are due to their different amounts of adsorbates on the samples. The ratios of exciton and trion emissions for these five samples are also shown in Fig. 4d and the variation tread is almost the same as their vacuum-level dependent PL intensities. Additionally, compared with that in air, the ratios of exciton and trion emissions are decreased in vacuum which further confirms that the amounts of adsorbates are highly related to the PL intensity and the ratios of exciton and trion emission intensities in MoS_2 and the optical performance of MoS_2 in vacuum are positively related to its crystal quality.

To clarify the most likely components of adsorbates in air and how the adsorbates contribute to the p doping effect on MoS_2, we have evaluated the charge transfer between adsorbates (O_2, N_2, OH^- and H_2O molecules) and MoS_2 by performing first-principle calculations as these three kinds of molecules are bountiful in air. We first consider the defects in MoS_2. As shown in Fig. S11, we consider four typical types of defects by using a 4×4 supercell of MoS_2 as the prototype: (1) a single S vacancy; (2) a single Mo vacancy; and (3) and (4) for two S vacancies at the same side and different sides. Our results show the single S vacancy is the most common defect with the lowest formation energies. Then we turn to focus on the charge transfer process between adsorbates and perfect (defective) MoS_2. The binding energy (E_b) of adsorbates A (O_2, N_2, OH^- and H_2O) on pristine or defective monolayer MoS_2 is given by

$$E_b = E(MoS_2 + A) - [E(MoS_2) + E(A)] \ (A = O_2, N_2, H_2O) \quad (2)$$

All energies are calculated within the same supercell for comparison. For the pristine MoS_2, three adsorption sites for O_2, N_2, OH^- and H_2O molecules are schematically shown in Fig. 5a,b, and their binding energies with MoS_2 are shown in Fig. 5c. The most favourable adsorption configurations for O_2, N_2 and OH^- are at B site, while for H_2O it is at A cite, which are in good accordance with former calculations[38]. For the defective MoS_2, we compare the adsorption energies of O_2, N_2, OH^- and H_2O molecules on its surface. Figure 5d shows O_2 molecule possesses the lowest adsorption energy (−3.25 eV), indicating O_2 molecules are the most likely component to be adsorbed on defective MoS_2. The O-H bond has a strong adsorption energy because it can form covalent bond on the Mo-edge[39], but the sample used in this work is S terminated[40]. Therefore, we only discuss the adsorption of O_2 molecules on the defect-sites of MoS_2. Figure 5e,f show the amounts of charge transfer between perfect (defective) MoS_2 and O_2, which are 0.002e and 1.025e, respectively. Obviously, the charge transfers can be greatly enhanced with defects introduced in MoS_2 and charges are extracted from defective MoS_2 by O_2 molecules due to its strong electronegativity. Thus, O_2 molecules play a major role in the p-doping effect for MoS_2. Moreover, to further confirm the doping effect of O_2 molecules, we anneal the samples at 400 °C in one hour with different oxygen atmosphere (20, 30, 40, 50 Torr) and find the introduction of O_2 indeed enhance the PL intensity of CVD grown monolayer MoS_2 samples, as shown in Fig. 6. The simulated charge transfer process is highly consistent with the experimental results. The more defects in CVD samples which act as the localization centre could form the stronger localized exciton and increase the radiative recombination of exciton of MoS_2.

Conclusion

In summary, we clarify the origin of the abnormally strong PL in CVD grown samples and attribute it to the p doping effects of adsorbates at the defect-sites. HRTEM and EDS are used to confirm more defects in CVD grown samples than that in ME samples, and the *in-situ* vacuum level dependent PL and Raman spectra, as well as the electrical performance confirms our proposal. The CVD samples under different grown conditions are expected with different crystal qualities, which show similar variation trends by different extent which further confirm the observed phenomenon. First principle calculations were carried out to investigate the charge transfer process between MoS_2 and adsorbates and clarify the p-doping effect of adsorbates due to the strong electronegativity of adsorbates. Such a p-doping effect from adsorbates reduces the concentration of excess electron in MoS_2 and contributes to the radiative recombination process of exciton. This work proposes a new vacuum technique to

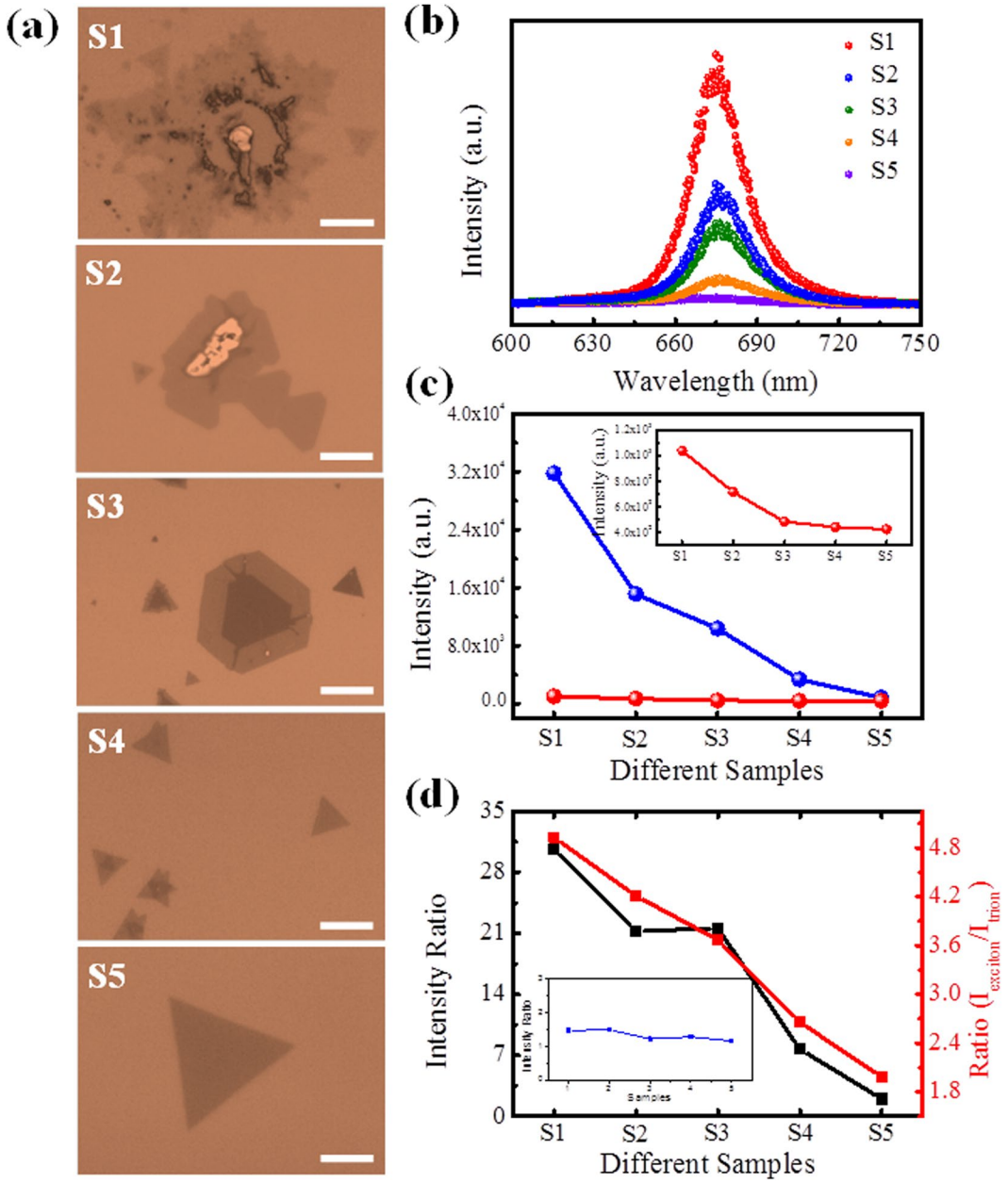

Figure 4. (**a**) Optical photos of CVD grown monolayer samples selected for PL measurement in (**b**), marked as S1, S2, S3, S4, S5. The scale bars shown in figures represent 15μm. (**b**) The corresponding PL spectra of CVD samples shown in (**a**). (**c**) The PL intensities of samples, shown in Figure (**b**), in air and in vacuum, respectively. The inset is the enlarged figure for the PL intensities in vacuum. (**d**) The ratios of PL intensities in air and vacuum for these five samples, and the intensity ratios of exciton and trion emissions for these five samples in air. The insert figure shows the intensity ratios of exciton and trion emission in vacuum.

evaluate the crystal quality and can guide the future works on the engineering of PL emission intensity on monolayer two-dimensional layered semiconductor materials.

Methods

Samples Preparation and Optical Characterization. Two groups of MoS_2 samples were used in this experiment: (1) monolayer MoS_2 exfoliated from nature MoS_2 crystals (from SPI), and (2) CVD grown monolayer MoS_2 (sulphur and MoO_3 powders are placed in furnace, with a SiO_2/Si substrate located face down above the MoO_3 powder). The growth temperature is at 650 °C and this temperature is kept with 15 min. Raman and PL spectra were conducted on Witec CRM 300 confocal Raman microscopy. The excitation laser was 532 nm laser with a spot size about 500 nm. The output power measured from the objective lens was controlled below 0.5 mW to avoid damaging and heating on samples. The accumulation time for PL and Raman spectra was 10 s. The Raman spectra were collected by 1800 g/mm grating while PL spectra were collected by 300 g/mm grating.

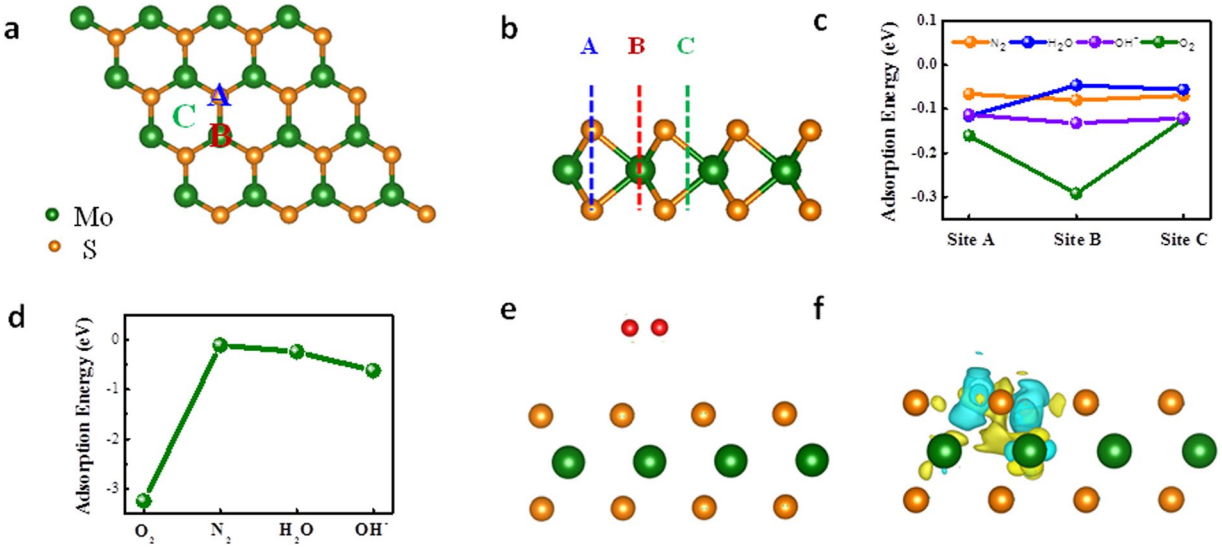

Figure 5. (**a**) Top and (**b**) side views of optimized structure of monolayer MoS_2. A, B, C represent the different adsorption sites of adsorbates. (**c**) The adsorption energies of O_2, N_2, H_2O and OH^- on A, B, C sites of pristine MoS_2. (**d**) The adsorption energies of O_2, N_2, H_2O and OH^- on defective MoS_2 with a S vacancy. (**e**) and (**f**) Show the charge density difference of O_2 molecule absorbed on pristine and defective 1 L MoS_2 with a single S vacancy, respectively. The positive and negative charges are shown in yellow and blue colors, respectively. Isosurface values are 7.5×10^{-2} e/Å^3 for (**e**) and 5×10^{-3} e/Å^3 (**f**).

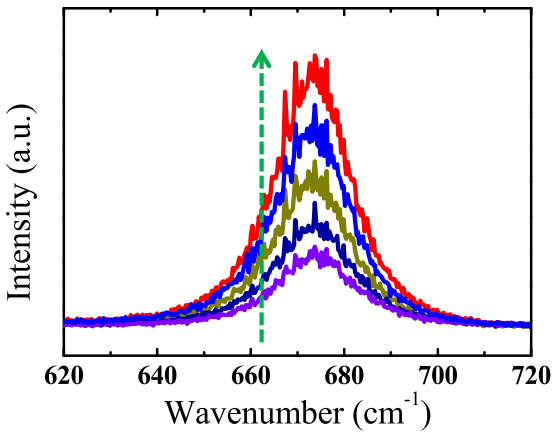

Figure 6. The PL spectra of annealed MoS_2 under different oxygen atmosphere. The arrow represents the increase of oxygen amounts. The purple line represents the PL spectra of pristine sample.

The size of the probe X-ray beam is 200 μm. For sample viewing, firstly, an optical image is taken by an external camera. Based on that optical image, we zoom in and position to roughly the area that we want. Then, similar to a SEM/EDX, a finely focused x-ray beam is used to create a secondary electron image for sample viewing, and actual positioning for interested analysis area.

Fabrication of Back-Gated MoS_2 Transistors. Both of these two groups of MoS_2 samples were deposited on 270 nm SiO_2/Si substrates. The devices were fabricated by standard electron beam lithography, followed by the thermal evaporation of Cr/Au electrode, and lift-off process. The electric measurement system was carried out using Agilent B1500A semiconductor analyzer. The vacuum level is set at 1×10^{-5} Torr.

First Principle Calculations. The first-principles calculations were realized based on the density functional theory (DFT), as implemented in the Vienna Ab initio Simulation Package (VASP)[41]. The exchange-correlation potential is chosen as generalized gradient approximation (GGA), formulated by Perdew-Burke-Ernzerhof (PBE) functional[42,43]. The cut off energy of 400 eV is used for the plane-wave expansion of valence electron-wave functions. To avoid artificial interaction between layers, a vacuum spacing of >15 Å is built. In the calculations, DFT-D2 method is employed to describe the long-range van der Waals interactions[44]. For both defects

identifications and gas molecules adsorptions on the monolayer MoS_2, the calculations were performed on a $4 \times 4 \times 1$ size of MoS_2 supercell, with Monkhorst-Pack k-point meshes of $7 \times 7 \times 1$[45]. The convergence criteria for energy and force are set to be 10^{-5} eV and 0.01 eV $Å^{-1}$, respectively. The amount of charge transfers between gas molecules and MoS_2 monolayer is estimated by using the Bader charge method.

References

1. Mak, K. F., Lee, C., Hone, J., Shan, J. & Heinz, T. F. Atomically thin MoS_2: A new direct-gap semiconductor. *Physical Review Letters* **105**, 136805 (2010).
2. Jian, S.-K., Jiang, Y.-F. & Yao, H. Emergent spacetime supersymmetry in 3D weyl semimetals and 2D dirac semimetals. *Physical Review Letters* **114**, 237001 (2015).
3. Wang, X. & Xia, F. Van der Waals heterostructures: stacked 2D mateirals shed light. *Nature materials* **14**, 264–265 (2015).
4. Mak, K. F. *et al*. Tightly bound trions in monolayer MoS_2. *Nature materials* **12**, 207–211 (2013).
5. Geim, A. K. & Grigorieva, I. V. Van der Waals heterostructures. *Nature* **499**, 419–425 (2013).
6. Urbaszek, B. & Marie, X. Valleytronics: Divice and polarize. *Nature Physics* **11**, 94–95 (2015).
7. Zeng, H., Dai, J., Yao, W., Xiao, D. & Cui, X. Valley polarization in MoS_2 monolayer by optical pumping. *Nature Nanotechnology* **7**, 490–493 (2012).
8. Cao, T. *et al*. Valley-selective circular dichroism of monolayer molybdenum disulphide. *Nature Communications* **3**, 887 (2012).
9. Xu, X., Yao, W., Xiao, D. & Heinz, T. F. Spin and pseudospins in layered transiton metal dichalcogenides. *Nature Physics* **10**, 343–350 (2014).
10. Sun, L. *et al*. Spin-orbit splitting in single-layer MoS_2 revealed by triply resonant Raman scattering. *Physical review letters* **111**, 126801 (2013).
11. Ma, T. *et al*. Edge-controlled growth and kinetics of single-crystal graphene domains by chemical vapor deposition. *Proceedings of the National Academy of Sciences* **110**, 20386–20391 (2013).
12. Wang, C. *et al*. Growth of millimeter-size single crystal graphene on Cu foils by circumfluence chemical vapor deposition. *Scientific Reports* **4**, 4537 (2014).
13. Park, W.-H., Jo, I., Hong, B. H. & Cheong, H. Controlling the ripple density and heights: a new way to improve the electrical performance of CVD-grown graphene. *Nanoscale* **8**, 9822–9827 (2016).
14. Kim, T.-Y. *et al*. Electrical properties of synthesized large-area MoS_2 field-effect transistors fabricated with inkjet-printed contacts. *ACS Nano* **10**, 2819–2826 (2016).
15. Park, J. *et al*. Thickness modulared MoS_2 grown by chemical vapor deposition for transparent and flexible electronic devices. *Applied Physics Letters* **106**, 012104 (2015).
16. Ji, Q. *et al*. Epitaxial monolayer MoS_2 on mica with novel photoluminsecence. *Nano Letters* **13**, 3870–3877 (2013).
17. Senthilkumar, V. *et al*. Direct vapor phase growth process and robust photoluminescence properties of large area MoS_2 layers. *Nano Research* **7**, 1759–1768 (2014).
18. U. M. Herb Goronkin, Proceedings of the Twenty-First INT Symposium on Compound Semiconductors, San Diego, California, USA (1994).
19. Chow, P. K. *et al*. Defect-induced photoluminescence in monolayer semiconducting transition metal dichalcogenides. *ACS Nano* **9**, 1520–1527 (2015).
20. Lee, Y. *et al*. Characterization of the structural defects in CVD-grown monolayered MoS_2 using near-field photoluminescence imaging. *Nanoscale* **7**, 11909–11914 (2015).
21. Nan, H. *et al*. Strong photoluminescence enhancement of MoS_2 through defect engineering and oxygen bonding. *ACS nano* **8**, 5738–5745 (2014).
22. Tongay, S. *et al*., Defects activated photoluminescence in two-dimensional semiconductors: interplay between bound, charged, and free excitons. *Scientific Reports* **3** (2013).
23. Zafar, A. *et al*. Probing the intrinsic optical qualityu of CVD grown MoS_2. *Nano Res* **5**, 1608–1617 (2017).
24. SuzukiR, S. M. *et al*. Valley-dependent spin polarization in bulk MoS_2 with broken inversion symmetry. *Nature Nanotechnology* **9**, 611–617 (2014).
25. Liu, Z. *et al*. Strain and structure heterogeneity in MoS_2 atomic layers grown by chemical vapor deposition. *Nature Communincations* **5**, 5246 (2014).
26. Jeon, J. *et al*. CVD growth of large-area two-dimensional MoS_2 films. *Nanoscale* **7**, 1688–1695 (2015).
27. Castellanos-Gomez, A. *et al*. Local strain engineering in atomically thin MoS_2. *Nano Letters* **13**, 5361–5366 (2013).
28. Wang, Y., Cong, C., Qiu, C. & Yu, T. Raman spectroscopy study of lattice vibration and crystallographic orientation of monolayer MoS_2 under uniaxial strain. *Small* **9**, 2857–2861 (2013).
29. Conley, H. J. *et al*. Bandgap engineering of strained monolayer and bilayer MoS_2. *Nano Letters* **13**, 3626–3630 (2013).
30. Hui, Y. Y. *et al*. Exceptional tunability of band energy in a compressively strained trilay MoS_2 sheet. *ACS nano* **7**, 7126–7131 (2013).
31. Chakraborty, B. *et al*. Symmetry-dependent phonon renormalization in monolayer MoS_2 transistor. *Physical Review B* **85**, 161403(R) (2012).
32. Attaccalite, C., Wirtz, L., Lazzeri, M., Mauri, F. & Rubio, A. Doped graphene as tunable electron-phonon coupling materials. *Nano Letters* **10**, 1172–1176 (2010).
33. Frey, G. L., Tenne, R., Matthews, M. J., Dresselhaus, M. S. & Dresselhaus, G. Raman and resonance Raman investigation of MoS_2 nanoparticles. *Physical Review B* **60**, 2883 (1999).
34. Mouri, S., Miyauchi, Y. & Matsuda, K. Tunable photoluminescence of monolayer MoS_2 via chemical doping. *Nano Letters* **13**, 5944–5948 (2013).
35. Siviniant, J., Scalbert, D., Kavokin, A. V., Coquillat, D. & Lascaray, J. P. Chemical equilibrium between excitons, electrons, and negatively charged excitons in semiconductor quantum wells. *Physical Review B* **59**, 1602 (1999).
36. Ross, J. S. *et al*. Electrical control of neutral and charged excitons in a monolayer semiconductor. *Nature Communications* **4**, 1474 (2013).
37. Vercik, A., Gobato, Y. G. & Brasil, M. J. S. P. Thermal equilibrium governing the formation of negatively charged excitons in resonant tunneling diodes. *Journal of Applied Physics* **92**, 1888–1892 (2002).
38. Yue, Q., Shao, Z., Chang, S. & Li, J. Adsorption of gas molecules on monolayer MoS_2 and effect of applied electric field. *Nanoscale Research Letters* **8**, 1 (2013).
39. Ghuman, K. K., Yadav, S. & Singh, C. V. Adosrption and dissociation of H_2O on monolayered MoS_2 edges: energetics and mechanism from ab Initio simultations. *The Journal of Physical Chemistry C* **119**, 6518 (2015).
40. van der Zande, A. M. *et al*. Grains and grain boudaries in hihgly crystalline monolayer molybdenum disulfide. *Nature. Materials* **12**, 554 (2013).
41. Kresse, G. & Joubert, D. From ultrasoft pesudopotentials to the projector augmented-wave method. *Physical Review B* **59**, 1758 (1999).
42. Perdew, J. P., Burke, K. & Wang, Y. Generalized gradient approximation for the exchange-correlation hole of a many-electron system. *Physical Review B* **54**, 16533 (1996).

43. Perdew, J. P., Burke, K. & Ernzerhof, M. Generalized gradient approximation made simple. *Physical Review Letters* **77**, 3865 (1996).
44. Grimme, S. Semiempirical GGA-type density functional constructed with a long-range dispersion correction. *Journal of Computational Chemistry* **27**, 1787–1799 (2006).
45. Monkhorst, H. J. & Pack, J. D. Special points for brillouin-zone integrations. *Physical Review B* **13**, 5188 (1976).

Acknowledgements

This research is supported by the National Research Foundation, Prime Minister's Office, Singapore under its NRF-ANR Joint Grant Call (NRF-ANR Award No. NRF2015-NRF-ANR000-CEENEMA), Singapore National Research Foundation under NRF RF Award No. NRF-RF2013-08. This work is partially supported by AFOSR grant 15IOA029.

Author Contributions

L.F. Sun and H.Y. Yang design the project and experiments. X.M. Zhang, X.F. Fan and S.A. Yang carried out the first principle calculations. F.C. Liu, S.J. Zheng, and Z. Liu fabricated the MoS_2 FETs and characterized them. Y.D. Shen and John T.L. Thong contributed to the set-up of facility for vacuum measurements. All authors contributed to the writing of the paper. The authors declare no competing financial interest.

Additional Information

Supplementary information accompanies this paper at https://doi.org/10.1038/s41598-017-15577-1.

Competing Interests: The authors declare that they have no competing interests.

Publisher's note: Springer Nature remains neutral with regard to jurisdictional claims in published maps and institutional affiliations.